Hydrol. Earth Syst. Sci. Discuss., 12, 2561–2605, 2015
www.hydrol-earth-syst-sci-discuss.net/12/2561/2015/
doi:10.5194/hessd-12-2561-2015

Hydrology and Earth System Sciences
Open Access
Discussions

Downscaling future precipitation extremes to urban hydrology scales using a spatio-temporal Neyman–Scott weather generator

H. J. D. Sørup[1,2], O. B. Christensen[2], K. Arnbjerg-Nielsen[1], and P. S. Mikkelsen[1]

[1]Urban Water Section, Department of Environmental Engineering, Technical University of Denmark, Lyngby, Denmark
[2]Danish Climate Centre, Danish Meteorological Institute, Copenhagen, Denmark

Received: 28 January 2015 – Accepted: 16 February 2015 – Published: 27 February 2015

Correspondence to: H. J. D. Sørup (hjds@env.dtu.dk)

Published by Copernicus Publications on behalf of the European Geosciences Union.

Abstract

Spatio-temporal precipitation is modelled for urban application at 1 h temporal resolution on a 2 km grid using a Spatio-Temporal Neyman–Scott Rectangular Pulses weather generator (WG). Precipitation time series for fitting the model are obtained from a network of 60 tipping-bucket rain gauges irregularly placed in a 40 by 60 km model domain. The model simulates precipitation time series that are comparable to the observations with respect to extreme precipitation statistics. The WG is used for downscaling climate change signals from Regional Climate Models (RCMs) with spatial resolutions of 25 and 8 km respectively. Six different RCM simulations are used to perturb the WG with climate change signals resulting in six very different perturbation schemes. All perturbed WGs result in more extreme precipitation at the sub-daily to multi-daily level and these extremes exhibit a much more realistic spatial pattern than what is observed in RCM precipitation output. The WG seems to correlate increased extreme intensities with an increased spatial extent of the extremes meaning that the climate-change-perturbed extremes have a larger spatial extent than those of the present climate. Overall, the WG produces robust results and is seen as a reliable procedure for downscaling RCM precipitation output for use in urban hydrology.

1 Introduction

Pluvial flooding of urban areas is often caused by very local extreme precipitation at sub-daily temporal scale (Berndtsson and Niemczynowicz, 1988; Schilling, 1991). Traditionally, historical gauge measurements of precipitation at minute-scale temporal resolution are thus used as input to design and analysis of urban water infrastructure (Mikkelsen et al., 1998; Madsen et al., 2009; Arnbjerg-Nielsen et al., 2013). Climate change is however expected to change the occurrence rate and magnitude of extreme events causing urban pluvial flooding (Fowler and Hennessy, 1995; Larsen et al., 2009; Olsson et al., 2009; Sunyer et al., 2014a), and high-resolution input time series repre-

HESSD
12, 2561–2605, 2015

senting future climates are therefore needed. Even though the overall qualitative features of precipitation are reproduced realistically by regional climate models (RCMs) (Christensen and Christensen, 2007) they are, however, not able to capture the very fine-scale spatio-temporal features of precipitation satisfactorily and yield output that is too spatially correlated (Tebaldi and Knutti, 2007; Gregersen et al., 2013). To overcome this, either dynamic downscaling with climate models has to operate at much finer scales (Kendon et al., 2014: Mayer et al., 2015) or further statistical downscaling of the climate model output has to be performed (Wood et al., 2004; Willems et al., 2012; Sunyer et al., 2012; Arnbjerg-Nielsen et al., 2013). Fine scale dynamic downscaling is computationally extremely expensive and statistical downscaling is therefore often favoured (Maraun et al., 2010). Several approaches exist within statistical downscaling, each with its pros and cons (Wilks and Wilby, 1999; Willems et al., 2012; Arnbjerg-Nielsen et al., 2013). In the present study a stochastic weather generator (WG) is used for statistical downscaling.

WGs can take different forms (Vrac et al., 2007; Burton et al., 2008; Arnbjerg-Nielsen and Onof, 2009; Chen et al., 2010; Cowpertwait et al., 2013) but they generally work by analysing observed precipitation (and possibly other weather related variables) and use the obtained statistics to create artificial stochastic precipitation (or weather) time series that replicate the behaviour of the observations with respect to these statistics (Maraun et al., 2010; Sunyer et al., 2012). Perturbation of the WG to yield output time series representing future climates is then possible by application of climate change factors calculated from output from RCMs (operation at too large space-time scales) to relevant parameters of the WG (that operates at the right space-time scale).

Several WGs exist that model precipitation as a stochastic point process where the given observations are considered single realisations of an underlying precipitation process (Waymire and Gupta, 1981). Rodríguez-Iturbe et al. (1987a, b) developed the stochastic point process models in a way to better characterise and describe the precipitation process at the event level. Implementations of the stochastic point process models for spatio-temporal precipitation seem to work satisfactorily at a temporal resolution of one hour or higher (Cowpertwait and O'Connell, 1997; Burton et al., 2008, 2010; Cowpertwait et al., 2013). Also, downscaling to finer resolution than one hour is inherently problematic as the scaling properties change below this point (Nguyen et al., 2002). Thus, for downscaling of extreme precipitation at sub-daily level and subsequent application of climate change signals from climate models, stochastic weather generators implementing stochastic point process models seem useful (Cowpertwait, 1998; Furrer and Katz, 2008; Hundecha et al., 2009; Verhoest et al., 2010; Sunyer et al., 2012). The trade-off is that the models do not involve rainfall movement and, hence that the spatio-temporal scale of the model has to be such that rainfall movement is not the main descriptor of the spatial rainfall pattern.

At the daily level, the Neyman–Scott Rectangular Pulses (NSRP) and the Spatio-Temporal Neyman–Scott Rectangular Pulses (STNSRP) models (Burton et al., 2008, 2010; Cowpertwait et al., 2013) have shown good skill in downscaling point precipitation extremes. This applies for individual gauges (Sunyer et al., 2012) as well as for spatially averaged precipitation covering large areas considered as having a uniform climate described by relatively few gauges (e.g. 5 gauges for a 4000 km^2 basin in the Pyrenees (Burton et al., 2010) and 3 gauges used to calibrate a regional model covering a catchment of 342 km^2 in the Basque Country, Cowpertwait et al., 2013). This is however inadequate in urban hydrology where the rainfall dynamics causing effects under study occur on much smaller time and space scales. In the present study, the STNSRP weather generator (WG) in the form of the software package RainSim (version 3.1.1, Burton et al., 2008) is used in a new, urban hydrology context focusing on much smaller space and time scales than what has been done in previous studies. It is fitted to hourly data from 60 rain gauges from a dense rain gauge network in Denmark and used to generate synthetic precipitation data series on an equally dense grid covering approximately 2400 km^2. The synthetic precipitation data is then evaluated with respect to its applicability for urban hydrological purposes. A 1 h temporal resolution on a 2 km grid is chosen as realistic and sufficient performance scales of the model for fine-scale precipitation data in urban hydrology. The evaluation of the WG is done from an engineering perspective with respect to its ability to reproduce rainfall features relevant for urban hydrological modelling. We will thus focus on:

- the WG's ability to produce realistic extreme event intensities at point scale,
- the WG's ability to reproduce the seasonal distribution of extreme events at point scale,
- the WG's ability to reproduce small scale spatio-temporal correlation structures of the extreme events.

This study uses the presented WG to analyse climate change in precipitation at scales comparable to the observational data sets traditionally used today for urban water infrastructure design and analysis. The WG is perturbed with climate change information obtained from a collection of temporal high resolution RCMs. Six RCM runs using three different RCMs, driven by three different GCMs and covering three different emission scenarios (ranging from average to very high emissions) are included in the analysis and four of the RCM runs are run as high resolution models at an 8 km grid. Finally, climate change at urban scale is assessed based on the perturbed WG output.

2 Data and weather generator

2.1 Data representing present conditions

The model area is a 40 × 60 km region covering the North-Eastern part of Zealand (Denmark) including Copenhagen, see Fig. 1. This study uses two different observational data sets; Table 1 summarises their main characteristics.

The area is highly urbanised and has a dense but irregular network of rain gauges designed and used for urban hydrology applications. The main observational precipitation data set, SVK (abbreviation for Spildevandskomiteen, the Water Pollution Committee of the Society of Danish Engineers) is obtained from this dense network of high-resolution

HESSD
12, 2561–2605, 2015

tipping bucket rain gauges (Jørgensen et al., 1998; Sunyer et al., 2013). Data from 60 stations that have been active between 2 and 34 years in the period 1979 and 2012 are included in the analysis; see Fig. 1 for locations within the study area. Figure 2 shows the temporal development of (top) the number of active stations and (middle) the average distance between nearest neighbouring stations through the measuring period, and Fig. 2 (bottom) shows the distribution of record lengths by 2012. Generally, there has been an increase in the number of stations and a densification of the network over the years. Some studies impose a minimum length of the time series to be included in regionalisation studies, e.g. Madsen et al. (2009), but in this study the cross-correlation is of key interest and hence all gauges are included in the analysis regardless of their record length. The original data resolution is 1 min and 0.2 mm but for the present study, data is aggregated to hourly time series. This data set is used to estimate (or calibrate, or fit) most of the parameters of the WG.

The second observational data set included in the analysis is referred to as the Climate Grid Denmark (CGD) (Scharling, 2012). It comprises spatially averaged daily data in a uniform 10 km grid for all of Denmark from 1989 to 2010 inclusive, cf. Fig. 1. This data is generated based on a national network of gauges/with 27 gauges within the study site (Scharling, 1999) and is only used to estimate the spatial component in the WG.

Finally, a third data set is the output from the applied weather generator (WG). A total of 10 data sets comprising sets of 50 years' time series in the 2 km grid (as shown on Fig. 1) are simulated as output from the WG. These data sets are used to corroborate the WG by refitting and rerunning it, evaluating the output variability and comparing the output statistics to those of observations.

2.2 Regional climate model data

Precipitation output from six different RCM runs is used in this study, see Table 2. Two of the model runs are identical to the ones used by Gregersen et al. (2013), namely the two SRES A1B scenarios driven by the RCM RACMO (version 2.1, van Meijgaard et al., 2008) and the RCM HIRHAM (version 5, Christensen et al., 2006), which are both driven by the GCM ECHAM5 (Roeckner et al., 2003) and are part on the ENSEMBLES project (van der Linden and Mitchell, 2009). Both have a spatial resolution of 25 km and a temporal output resolution of 1 h. These were the two ENSEMBLES runs we had available at true 1 h resolution. The more generally available data series with only daily maximum 1 h intensity are not sufficient for the employed downscaling procedure. The four other simulations used in this study are run with the RCM HIRHAM driven by the GCM EC-EARTH (Hazeleger et al., 2012) and the RCM WRF (Skamarock et al., 2005) driven by the GCM NorESM (Bentsen et al., 2013). The four simulations use the RCP 4.5 and RCP 8.5 scenarios (van Vuuren et al., 2011), see Table 2. The resolution of these simulations is 8 km and 1 h (Mayer et al., 2015). The simulations were carried out as part of the research project RiskChange (www.riskchange.dhigroup.com). The SRES A1B and RCP 4.5 scenarios are considered comparable moderate forcing scenarios whereas the RCP 8.5 scenario is a very strong forcing scenario.

As in Gregersen et al. (2013), climate change is considered uniform for all land cells over Denmark; this results in 87 considered grid cells for the ENSEMBLES simulations and 648 for the RiskChange simulations.

2.3 Weather generator

The RainSim WG describes the spatio-temporal rain field as discs of rain (rain cells) with uniform rain intensity that temporarily occur and overlap in space and time to produce output that realistically describe the statistical properties of precipitation. As the calibration data set consists of point observations, the time series from the simulations are not grid cell averages but strictly comparable to what a gauge would have measured if present in a grid point. Seven parameters describe the WG (Burton et al., 2008, 2010):

- λ^{-1}, the mean waiting time between storm origins (in h)
- β^{-1}, the mean waiting time for rain cell origins after storm origin (in h)

- η^{-1}, the mean duration of rain cells (in h)
- ρ, the spatial density of rainfall cell centres (cells per km^2)
- ξ^{-1}, the mean intensity of the rain cells (in mm h^{-1})
- γ^{-1}, the mean radius of the rain cells (in km)
- Φ, the non-homogeneous intensity scaling field describing how the mean monthly rainfall intensity varies in space within the model area (–)

A uniform Poisson process governed by λ describes the storm occurrences. For each storm a random number of rain cells are produced, which occur at independent time intervals after the storm origin and where the time intervals follow an exponential distribution with parameter β. A uniform spatial Poisson process governed by ρ describes the density of the rain cells in space. The cell radii are randomly drawn from an exponential distribution described by γ, and the duration and intensity of each rain cell is independent and follows an exponential distribution with parameters η and ξ, respectively. The rain intensity at a given point is therefore the sum of all overlapping rain cell intensities at a given time (Burton et al., 2008, 2010).

The non-homogeneous intensity scaling field, Φ, is a proxy for the spatial variation of mean monthly precipitation and is used for relative scaling of the precipitation in space; for this study it is interpolated from the CGD data set using inverse distance weighting. Regional modelling of short-duration extreme precipitation for Denmark using the SVK data set has shown that the only significant parameter that can explain the geographical variation of point extremes statistically is the corresponding mean annual precipitation (Madsen et al., 2002, 2009). Thus, taking Φ as the only spatially varying parameter in the WG, and as such the only parameter describing spatial differences within the WG, is considered to be an acceptable approximation. The actual spatial variation of mean monthly precipitation calculated from the CGD data set is considerable (see Fig. 3), even though the model area is small in size and relatively flat. Especially in June and

HESSD
12, 2561–2605, 2015

July there is a clear North–South gradient with 75–80 mm month^{-1} in the North of the area and 55–60 mm month^{-1} in the South.

3 Methodology

3.1 Fitting of the weather generator

RainSim is fitted to daily and hourly statistics for each calendar month from the observed time series (SVK) to best reproduce features at both hourly and daily levels, as described by Burton et al. (2008, 2010). A custom weighing scheme is used to support the features of rainfall that are important in the context of the present study. RainSim uses the Shuffled Complex Evolution fitting algorithm in combination with an objective function that normalises the fitting statistics (to avoid bias) for optimisation; furthermore, the algorithm is run thrice to avoid sub-optima (Burton et al., 2008). The statistics used for fitting the WG are:

- the mean daily precipitation intensity from the individual gauges (24 h mean);
- the variance of the intensity of the daily and hourly observations from the individual gauges (1 and 24 h variance);
- the skewness of the intensity of the daily and hourly observations from the individual gauges (1 and 24 h skewness);
- the probability of dry days and of dry hours based on the observations from the individual gauges and with thresholds of 1.0 and 0.1 mm respectively as suggested by Burton et al. (2008);
- the lag-1 auto-correlation of the hourly precipitation intensity calculated from the observations at the individual gauges;

HESSD
12, 2561–2605, 2015

– the cross-correlation between observations of hourly precipitation intensity at the individual gauges.

The chosen weighing scheme (see Table 3) favours the higher order moment statistics variance and skewness over the mean as the extreme characteristics of the simulated precipitation is prioritised. Furthermore, the cross-correlation and auto-correlation are given high weights to ensure a realistic representation of the spatio-temporal extent of the simulated precipitation. The different observation time series are furthermore weighted relative to each other according to the effective length of the time series to give more weight to longer time series. This is done to increase the data basis for cross-correlation analysis, utilising that a great deal of the short time series are from recent years and thus overlap in time, see Fig. 2.

The standard fitting bounds suggested by Burton et al. (2008) are applied in the fitting procedure to ensure that the WG is fitted with values that are considered realistic by the model developers for a North European climate.

3.2 Evaluation of simulated time series

For evaluation of all realisations of the WG the 60 grid cells closest to the observational gauges are extracted and evaluated point-wise with respect to all the fitting statistics as recommended by Burton et al. (2008). Furthermore, the WG is refitted to the simulated data sets to evaluate if the realisation is representative and results in model parameters that are comparable to the parameters estimated from the SVK observational data set.

Ten realisations of the WG, named WG1 to WG10, are used in this study.

3.3 Perturbation of the weather generator with climate change signals

The fitted WG is perturbed with climate change signals by application of climate change factors, $\alpha_{i,j,k}$'s, to the key statistics, $Y_{i,j,k}^{\text{Present}}$'s, calculated from the SVK data set and used to fit the original WG for the present climate. In this manner new key statistics are produced for the future climate, $Y_{i,j,k}^{\text{Future}}$'s, as (Fowler et al., 2007)

$$Y_{i,j,k}^{\text{Future}} = \alpha_{i,j,k} Y_{i,j,k}^{\text{Present}}. \quad (1)$$

One climate change factor is calculated for each statistic, i, for each month, j, for each RCM, k. The change factors are calculated using the methodology introduced by Burton et al. (2010) which includes transformations that ensure that the bounded statistics (probabilities of dry days and hours and auto-correlation) stays within their prescribed boundaries. No change factor is calculated for the cross-correlation as this statistic is described poorly by the RCMs (Gregersen et al., 2013).

3.4 Evaluation of extremes

Gregersen et al. (2013) compare extreme precipitation observations with RCM output. One issue is the difference in absolute magnitude of the extremes, which can partly be explained by the inherent difference between gridded data and point observations; another issue is the spatial correlation structure of the extremes, where extremes calculated from RCM output have much too large spatial correlation distances at the sub-daily time scale. In this study, a simulated data set will be considered better than using RCM data directly for the specified purpose if it better resembles the observations with respect to both the absolute magnitude and the spatial correlation structure of the extremes.

The statistics used in this study to evaluate the WG's performance with respect to simulating extreme precipitation are based on the identification of independent rainfall events, as done when estimating intensity-frequency-duration relationships, see e.g. Madsen et al. (2002). Individual events are separated by dry periods equal to or longer than the chosen event duration (i.e. 1 h events have at least 1 h of dry weather between them and 24 h events have at least 24 h of dry weather between them) and the maximum averaged event intensities over the chosen durations are noted. Furthermore, the Peak over Threshold (POT) approach from Mikkelsen et al. (1996) and

HESSD
12, 2561–2605, 2015

Madsen et al. (2002) is adopted with a global constant intensity threshold (i.e. Type I censoring) to derive the extreme event intensities for each gauge/grid point. In this study, extreme precipitation events are evaluated for 11 distinct durations of between 1 and 120 h with thresholds ranging from 7.6 to 0.34 $\mathrm{mm\,h^{-1}}$ (the same as used by Gregersen et al. (2013) for the SVK data set). Three different event-based indices of extreme precipitation are evaluated as explained below.

3.4.1 Extreme event statistics

The return period of extreme events extracted from an observed or simulated rainfall time series is calculated using the California plotting position formula:

$$T_m = \frac{T_{\mathrm{obs}}}{m}, \tag{2}$$

where T_m is the return period of the event (years) with rank m and T_{obs} is the observation period (years) of the time series. T_m is obviously affected by sampling variability and is biased, especially for large return periods. There are more elaborate methods to estimate T_m than Eq. (1), but we use Eq. (1) here because it allows for comparing extreme value curves from multiple sites (including sampling variability and spatial variability) in a straightforward way.

A Generalised Pareto Distribution is fitted to extremes from every single time series:

$$z_T = z_0 + \mu \frac{1+\kappa}{\kappa}\left(1 - \left(\frac{1}{\lambda T}\right)^{\kappa}\right), \tag{3}$$

where:

- z_T is the intensity for extreme event with return period T;
- z_0 is the threshold;
- μ is the mean intensity of the extreme events;

HESSD
12, 2561–2605, 2015

- λ is the mean number of extremes per year;
- κ is the shape parameter;
- T is the return period.

Based on $z(T)$'s intensity-duration-frequency curves are calculated for each data set.

For the climate change scenarios, change factors for the intensity of the extreme events are calculated as a function of the return period for different T-year event durations. This is done as a simple ratio between the present and future levels for a given return period as

$$CF_T = \frac{z(T)^{\text{future}}}{z(T)^{\text{present}}}. \quad (4)$$

3.4.2 Seasonality of extreme events

The seasonality of the extreme events is determined to further evaluate the realism of the behaviour of the WG. This is done to evaluate whether the WG data set constructed with individual monthly model parameters results in a realistic distribution of the extremes throughout the year. The determination is in practice performed by counting the number of extremes from the POT analysis that occur within each month for the SVK and WG data sets. These are then normalised and compared with a χ^2 test where the normalised counts C for the SVK data act as the expected values for the WG data set and where the summation is done over months giving a test statistic x:

$$x = \sum_{i=1}^{12} \frac{\left(C_i^{\text{WG}} - C_i^{\text{SVK}}\right)^2}{C_i^{\text{SVK}}} \quad (5)$$

x then follows a χ^2-distribution with $(12-1)(2-1) = 11$ degrees of freedom.

HESSD
12, 2561–2605, 2015

3.4.3 Unconditional spatial correlation of extremes

The unconditional spatial correlation, ρ, between the intensities of extreme events that are considered concurrent at different sites A and B is estimated. The methodology follows Mikkelsen et al. (1996) with the ith extreme intensity Z_{Ai} measured at site A being concurrent with the jth extreme event Z_{Bj} measured at site B if Eq. (6) is fulfilled. In this framework the precipitation process is considered to generate random occurrences of precipitation that are treated as correlated random variables, Z_A and Z_B, and two events are considered concurrent if they are overlapping in time or at most separated by a lag time Δt, which is introduced to account for the travel time of rain storms between sites.

$$\{Z_{Ai}, Z_{Bj}\} : \left[t_{si} - \frac{\Delta t}{2}, t_{ei} + \frac{\Delta t}{2}\right]_A \cap \left[t_{sj} - \frac{\Delta t}{2}, t_{ej} + \frac{\Delta t}{2}\right]_B \neq \varnothing \tag{6}$$

Here, t_s is the start times of the events and t_e is the end time of events. A lag time of $\Delta t = 11\,\mathrm{h}$ + the duration of the event is adopted in accordance with Gregersen et al. (2013). The introduction of this lag time, in combination with lack of knowledge of the movement direction of precipitation, implies that an individual event at one site can be correlated to more than one event at another site.

The unconditional covariance is then estimated by also accounting for non-concurrent extreme events at the two sites as:

$$\mathrm{cov}\{Z_A, Z_B\} = \mathrm{cov}\{\mathrm{E}\{Z_A|U\}, \mathrm{E}\{Z_B|U\}\} + \mathrm{E}\{\mathrm{cov}\{Z_A, Z_B|U\}\} \tag{7}$$

with U being a boolean operator taking the value of $U = 1$ if events are concurrent and $U = 0$ otherwise. Finally, the unconditional correlation is obtained by division of Eq. (7) with the sample SDs of the two sites (Mikkelsen et al., 1996):

$$\rho_{AB} = \frac{\mathrm{cov}\{Z_A, Z_B\}}{\sqrt{\mathrm{var}\{Z_A\}\mathrm{var}\{Z_B\}}} \tag{8}$$

HESSD
12, 2561–2605, 2015

The unconditional correlation values are grouped together in bins where the distance between the points considered are approximately the same, and an exponential model is fitted to describe the unconditional correlation's dependence on distance between sites using the e-folding distance measure as proposed by Gregersen et al. (2013).

4 Results and discussion

4.1 Fitting the weather generator

The WG converges to an optimum fit for the SVK and CGD data for all calendar months, resulting in a WG that is able to simulate realistic rainfall fields all year round. The parameter estimates (cf. Sect. 2.3) for the model fitted to SVK data, the parameter estimates for the model refitted to the 10 realisations of the WG (WG1 – WG10) and the used boundary values are given in Fig. 4. All parameters vary over the course of the year, some more smoothly than others. Note that the β parameter (the parameter controlling the arrival time of cells after a storm origin) is constrained at its prescribed minimum value for four months (February, September, October and December). However, rain events can easily last for several days at these times of the year in Denmark, and this fitting artefact is therefore considered to have limited influence on those features of rainfall, which are of interest for this study. Figure 4 shows that all the refitted values are different and especially the β parameter does not always seem to follow the same structural pattern as for the SVK data set. As β^{-1} controls the arrival time of cells after storm origin it will be heavily dependent on the actual realisation of weather from the WG and this is not considered to be important for the realised extreme events. The ξ parameter seems to be slightly biased in the same direction for all WGs. ξ^{-1} controls the mean intensity of the rain cells and the difference in fit suggests that the rain in the WG data sets are slightly more intense during summer than what is seen in the SVK data set. Generally, the WG data sets however represent the SVK data set well.

HESSD
12, 2561–2605, 2015

The fitting statistics (cf. Sect. 3.1) resulting from the direct analysis of the observations (SVK data set) and the simulations (WG data sets that are simulated based on fitting the WG to the SVK and CGD data) are compared in Fig. 5. Generally, the fit seems reasonable for all variables. For the moment statistics the WG data sets seem to be unable to reproduce the highest observed values (Fig. 5a–e), but for the bulk of observational points the fit is very good. The lag-1 auto-correlation and the probabilities of dry days and hours all seem to be fitted well. Also, it seems that none of the WG realisations performs differently than the others with respect to reproduction of the fitting statistics.

The cross correlation of the 1 h intensities is shown on Fig. 6 for each month of the year. The 10 WG data sets seem to reflect the overall behaviour of the SVK data set very well and also capture most of the variability seen in the SVK data set. The very low correlations observed in the SVK data set for some "traces" of points, especially in March, October and November, are due to some time series only overlapping for very short time periods in recent years where the number of stations has increased dramatically (see Fig. 2); hence the correlation is depending on only very few precipitation events. There is no evidence of a systematic pattern in these readings. Again, the difference between different WG realisations is very limited.

From Figs. 5 and 6 the WG fit is considered satisfactory given the complex data set used and the purpose of this study. For analysis of extremes at event level this WG reproduces the features expected to have the highest influence on the produced extremes well.

4.2 Evaluation of extremes for present climate conditions

For durations of 1 to 120 h the extreme events are extracted from the SVK data set at each gauge and from the WG data sets in each grid cell closest to the SVK observation points and ranked according to return period (Eq. 2). Figure 7 shows intensity-duration-frequency curves estimated for WG realisation along with the SVK data set. For both

HESSD
12, 2561–2605, 2015

50 and 10 year events the WG data sets result in comparable extreme intensity values for all considered durations.

Figure 8 shows that the seasonal distribution of these extreme events is captured very well by the considered grids from the simulated WG data sets for all considered event durations. The χ^2 tests furthermore confirm that there are no significant differences between distributions for the WG and the SVK data sets for all event durations.

Figure 9 shows the unconditional spatial correlation for the SVK and for the selected WG grid points calculated according to Eq. (8) and grouped in selected bins. Table 4 furthermore compares the e-folding distances based on the fitted exponential models with a set of values calculated from RCM data representing a slightly larger area, taken from Gregersen et al. (2013).

Gregersen et al. (2013) show, using data from the whole of Denmark (range 0–350 km), that the spatial correlation pattern is not the same when considering output from climate models compared to SVK data as the climate model output maintains too long spatial correlation lengths at scales below approximately 150 km and 12 h (see Table 4). Both Fig. 9 and Table 4 indicate that the WG better reproduces the spatial correlation pattern of the SVK data within the spatial range (0–60 km) covered by the observations included in this study. The e-folding distances computed in this study for the SVK data set are somewhat lower than the ones calculated by Gregersen et al. (2013). This is a consequence of inclusion of fewer gauges and, most importantly, that the time series in the SVK data set for this study have been aggregated into hourly time series prior to the smoothing and POT analysis. Gregersen et al. (2013) conducted the smoothing and POT analysis directly on the original time series that have a one-minute resolution. The WG data sets represent the space-time features of precipitation of crucial importance for urban hydrology applications much better than the climate model output; the WG data set is considered realistic at this small-scale spatio-temporal resolution.

Overall, the results show that the WG is able to realistically simulate extreme precipitation statistics down to the hourly scale at a 2 × 2 km spatial resolution.

HESSD
12, 2561–2605, 2015

4.3 Perturbation of the weather generator with climate change signals from RCMs

As the different realisations of the WG produce similar weather, only one 30 years realisation is used for perturbation with climate change signals from each of the RCMs. Furthermore, all grid cells are used for both present and future evaluations as no comparisons are made to the observational data.

For each RCM run and each statistic the climate change factors, $\alpha_{i,j,k}$'s, are calculated. They are primarily above 1 for the moment derived statistics (Fig. 10a–e) but the different RCM runs appear different. For the 24 h mean (Fig. 10a) the $\alpha_{i,j,k}$'s are mostly above 1 with all RCM runs showing some months with values below 1 in an unsystematic pattern. For both the 24 and 1 h variances (Fig. 10b and d) the number of RCM runs and months that show a decrease is very limited and in general the variance will increase for all seasons. The HIRHAM RCP 8.5 simulation differs from the other RCM runs with very high $\alpha_{i,j,k}$'s for the summer months. The 24 and 1 h skewness (Fig. 10c and e) show more clear seasonality than the mean and variance with higher $\alpha_{i,j,k}$'s from May to September for all RCM runs clearly indicating a shift in the distribution of precipitation intensities towards more extremes. Again the HIRHAM RCP 8.5 run stands out with very high $\alpha_{i,j,k}$'s for the 1 h skewness for most of the year. This means that the extreme precipitation intensities are expected to be higher during summer and especially the sub-daily extremes for the HIRHAM RCP 8.5 perturbation could have very high intensities as a combination of a large increase in both variance and skewness will result in many severe precipitation events with a high mean intensity.

For the lag-1 h auto-correlation (Fig. 10h) the $\alpha_{i,j,k}$ are mostly below 1 indicating more variations from one hour to the next and thus a possibility of more abrupt changes in the rainfall at the hourly level. For the probability of dry days and dry hours (Fig. 10f and g) the pattern is less clear. The RCM simulations show some variation around 1 (approximately between 0.7 and 1.7) but do not agree with respect to season of these changes or their relative magnitude. This suggests that future rainfall will follow the same overall patterns as today but as all RCM runs have months with $\alpha_{i,j,k}$ below 1 there will also be more severe periods since the precipitation is concentrated on fewer days and hours. For instance, the peaks for the WRF RCP 8.5 perturbation in August for both probability of dry days and hours (Fig. 10f and g) in combination with the increases in variance and skewness (Fig. 10b–e) are expected to result in very severe extremes as the increased rainfall amount is expected to occur on fewer days. All in all, the $\alpha_{i,j,k}$'s indicate that for all RCM runs there will be more rainfall on average and it will be more variable resulting in more (and more severe) extremes events. This is in accordance with general findings from studies based on direct output from RCMs (Christensen and Christensen, 2007; Sunyer et al., 2014b).

4.4 Changes in climate changed extremes from the weather generator

Calculating the climate change factors, CF's (Eq. 4), from the perturbed and original WG using the T-year event estimates calculated with Eq. (3) shows that despite the differences observed in the $\alpha_{i,j,k}$ for the input statistics (Fig. 10), the perturbation schemes based on RCM simulations modelling comparable climate change (HIRHAM SRES A1B, RACMO SRES A1B, HIRHAM RCP 4.5 and WRF RCP 4.5) result in similar changes to extremes after downscaling with the WG (Fig. 11). Clearly, and as expected from the results in Fig. 10, the HIRHAM RCP 8.5 perturbed WG results in a much more severe change in extreme precipitation than the other perturbation schemes for both 10 and 100 year return periods. It is interesting that the WG perturbed with HIRHAM SRES A1B results in a rather stable CF in the range 1.35–1.55 with seemingly little dependence on return period and event duration, The WGs perturbed with RACMO SRES A1B, HIRHAM RCP 4.5 and WRF RCP 4.5 show similar CF values that are higher for 100 year extremes than for 10 year extremes but still not depend significantly on the event duration.

Both the HIRHAM RCP 8.5 and WRF RCP 8.5 perturbed WGs yield CF values that depend on the event duration with higher CF for short duration precipitation extremes. This indicates that this high-end scenario is changing the climate more drastically than

HESSD
12, 2561–2605, 2015

the more moderate scenarios (SRES A1B and RCP 4.5) and that the observed extreme effects are not linearly scalable from moderate to high end scenarios. For event durations above 48 h the different WGs yield similar CF's, but surprisingly the high-end scenario WRF RCP 8.5 perturbation scheme results in the smallest CF for the long duration events. This may indicate that the direct output from the RCMs underestimate the changes occurring at high spatio-temporal resolutions.

Despite the observed differences between WGs perturbed with different RCM runs and different forcing scenarios the results show an upwards change for all event durations (see Fig. 11). The change seems to increase with the return period with a projected change factor in the order of 1.2–1.3 for $T = 10$ years and 1.4–1.5 for $T = 100$ years for the moderate scenarios (SRES A1B and RCP 4.5). Furthermore, the RCP 8.5 scenario perturbed WG runs suggest that short duration extreme events become relatively more severe compared to the WG runs perturbed with the other, moderate forcing scenarios.

4.5 Unconditional spatial correlation of climate changed T-year events

All the perturbed WG runs produce T-year precipitation events with reasonable spatial correlation structure (Fig. 12, Table 5) includes calculated e-folding distances and it is noteworthy that the e-folding distance for present conditions is somewhat shorter for the full WG data set compared to the sub sets closest to the observations shown in Fig. 9. The HIRHAM RCM and WRF RCM perturbed WG runs present similar results for all event durations whereas the RACMO SRES A1B perturbed WG run yield slightly larger correlations lengths for the very short durations (Fig. 12a). Generally, all the perturbed WG runs have larger correlation lengths than for the present climate, suggesting that the WG implicitly expects that more severe events on average also results in events with a larger spatial extent. This behaviour has recently been observed by Kendon et al. (2014) using a high resolution regional climate model (1.5 km resolution). This difference, however, is limited, and in general the WG produces extremes with a spatial extent much closer to that of observations than RCMs. Online Resource 1 includes an animation of extreme precipitation events generated directly as output from the 25 km resolution RCM HIRHAM SRES A1B, the 8 km resolution RCM HIRHAM RCP 4.5 and the 2 km WG evaluated in this study. From these it is clear that the small-scale variability is much more pronounced for the WG output than for the output of the RCMs, but also that the WG output lacks rainfall movement. At the hourly scale this is not a problem for a catchment of the size presented in the Online Resource (same as shown in Fig. 1).

Only few apparent effects are observed with respect to choice of RCM, GCM and RCM spatial resolution and it is not possible to detect any systematic patterns. The WG seems to produce robust results with respect to change in extreme precipitation due to climate change that are similar for similar climate forcing scenarios.

5 Conclusions

Precipitation time series based on high-resolution gauge measurements are presently used as input to design and analysis of urban water infrastructure, and time series representing future climates are needed in the future. Current RCMs operating at 25 and even 8 km spatial scales however yield too spatially correlated output that poorly represents the fine-scale precipitation features relevant for urban hydrology. The study indicate that statistical downscaling of precipitation output from RCMs using a stochastic weather generator (WG) is therefore a better solution.

This study demonstrates that the chosen Spatio-Temporal Neuman–Scott Rectangular Pulses weather generator (WG) fitted to a dense network of 60 rain gauges in a 40 by 60 km region simulates realistic extreme precipitation of relevance to urban hydrology. Output is generated at the 1 h temporal scale at a 2 km spatial grid, which is finer than what previous studies using this WG have focused on. Even though urban hydrology literature claims that rain data are ideally needed at a time scale of minutes, the hourly scale chosen here can still be of much use when assessing climate change impacts in urban hydrology as it is much finer than what regional climate models can currently provide.

The WG generally reproduces statistics of the observations such as mean, variance and skewness of the rainfall intensity distribution well at both the hourly and daily levels. It also produces realistic levels of lag-1 auto-correlation, cross-correlation between output at different grid points and probabilities of dry days and hours. Evaluating the WG from an urban hydrological engineering perspective yields the following conclusions:

– The extreme events of the simulated time series show realistic levels of intensity as well as a reasonable spatial variability for the full 60 × 40 km model area. Thus, the WG handles the large data set of spatially distributed observational input in a robust manner.

– The seasonal distribution of the extremes are not significantly different in the generated WG data sets compared to the observed SVK data set, implying that the applied procedure of individual monthly model fits results in a realistic seasonal behaviour of the WG.

– The spatial extent of the extreme events in the WG data set, as evidenced by the unconditional spatial correlation of extremes, is close to that of the observational SVK data set with e-folding distances in the same order of magnitude. This is much better than what is observed for Regional Climate Model (RCM) output at 25 and 8 km grid scale in previous studies.

This indicates that the WG is a good way to downscale spatio-temporal precipitation output from RCMs to relevant urban scales and that the simulated output can be used directly as input to urban hydrological models.

Output from six different RCM runs representing average to high emission scenarios are used to perturb the WG for different possible future climate scenarios. Two have a 25 by 25 km spatial resolution and four have a very high 8 by 8 km spatial resolution, and all RCM data sets are available at hourly temporal resolution. A clear increase in the magnitude of extreme precipitation is observed for all climate change perturbations of the WG.

HESSD
12, 2561–2605, 2015

This study highlights that different RCMs run with the same greenhouse gas emission scenario can result in different precipitation output and hence different CFs for perturbation of the WG. Despite these observed differences, downscaling with the WG results in similar extreme precipitation behaviour for similar emission scenarios.

Most perturbed WGs confirm that there is a more severe climate change signal for extreme events. The two WGs perturbed by the RCP 8.5 scenario show a more severe climate change signal for short-duration events. However, this finding is not shared by the other emission scenarios, suggesting that extreme precipitation at T-year event level is not scalable between emission scenarios. The spatial correlation structure of the WG output is slightly altered by the perturbation indicating a built-in correlation between intensity and spatial extent and suggesting that precipitation extremes in a future climate may have larger spatial extent than extremes in the present climate.

The Supplement related to this article is available online at doi:10.5194/hessd-12-2561-2015-supplement.

Acknowledgements. This work was carried out with the support of the Danish Council for Independent Research as part of the project "Reducing Uncertainty of Future Extreme Precipitation", contract no. 09-067455. The observational SVK data set was provided by the Water Pollution Committee of the Society of Danish Engineers. The Climate Grid Denmark (CGD) is a commercial product made freely available for research by the Danish Meteorological Institute. The authors also thank the Royal Netherlands Meteorological Institute, KNMI, and Erik van Meijgaard who kindly provided the RACMO data in a temporal resolution of 1 h, although this was outside the agreement of the ENSEMBLES project. The high resolution regional climate model runs were carried out as part of the project RiskChange funded by the Danish Council for Strategic Research, contract no. 10-093894 (http://riskchange.dhigroup.com).

References

Arnbjerg-Nielsen, K. and Onof, C.: Quantification of anticipated future changes in high resolution design rainfall for urban areas, Atmos. Res., 2, 350–363, doi:10.1016/j.atmosres.2009.01.014, 2009.

Arnbjerg-Nielsen, K., Willems, P., Olsson, J., Beecham, S., Pathirana. A., Gregersen, I. B., Madsen, H., and Nguyen, V.-T.-V.: Impacts of climate change on rainfall extremes and urban drainage systems: a review, Water Sci. Technol., 68, 16–28, doi:10.2166/wst.2013.251, 2013.

Bentsen, M., Bethke, I., Debernard, J. B., Iversen, T., Kirkevåg, A., Seland, Ø., Drange, H., Roelandt, C., Seierstad, I. A., Hoose, C., and Kristjánsson, J. E.: The Norwegian Earth System Model, NorESM1-M – Part 1: Description and basic evaluation of the physical climate, Geosci. Model Dev., 6, 687–720, doi:10.5194/gmd-6-687-2013, 2013.

Berndtsson, R. and Niemczynowicz, J.: Spatial and temporal scales in rainfall analysis: some aspects and future perspectives, J. Hydrol., 100, 293–313, doi:10.1016/0022-1694(88)90189-8, 1988.

Burton, A., Kilsby, C. G., Fowler, H. J., Cowpertwait, P. S. P., and O'Connel, P. E.: RainSim: a spatial temporal stochastic rainfall modelling system, Environ. Modell. Softw., 23, 1356–1369, doi:10.1016/j.envsoft.2008.04.003, 2008.

Burton, A., Fowler, H. J., Kilsby, C. G., and O'Connell, P. E.: A stochastic model for the spatial-temporal simulation of nonhomogeneous rainfall occurrence and amounts, Water Resour. Res., 46, W11501, doi:10.1029/2009WR008884, 2010.

Chen, J., Brissette, F. P., and Leconte, R.: A daily stochastic weather generator for preserving low-frequency of climate variability, J. Hydrol., 388, 480–490, doi:10.1016/j.jhydrol.2010.05.032, 2010.

Cowpertwait, P. S. P.: A Poisson-cluster model of rainfall: high-order moments and extreme values, Proc. Roy. Soc. A-Math. Phy., 454, 885–898, doi:10.1098/rspa.1998.0191, 1998.

Cowpertwait, P. S. P. and O'Connell, P. E.: A Regionalised Neyman-Scott Model of Rainfall with Convective and Stratiform Cells, Hydrol. Earth Syst. Sci., 1, 71–80, doi:10.5194/hess-1-71-1997, 1997.

Cowpertwait, P., Ocio, D., Collazos, G., de Cos, O., and Stocker, C.: Regionalised spatiotemporal rainfall and temperature models for flood studies in the Basque Country, Spain, Hydrol. Earth Syst. Sci., 17, 479–494, doi:10.5194/hess-17-479-2013, 2013.

Christensen, O. B. and Christensen, J. H.: A summary of the PRUDENCE model projections of changes in European climate by the end of the century, Climatic Change, 81, 7–30, doi:10.1007/s10584-006-9210-7, 2007.

Christensen, O. B., Drews, M., Christensen, J. H., Dethloff, K., Ketelsen, K., Hebestadt, I., and Rinke, A.: The HIRHAM Regional Climate Model, version 5(β), Danish Meteorological Institute, Copenhagen, Denmark, Technical Report 06–17, 2006.

Fowler, A. M. and Hennessy, K. J.: Potential impacts of global warming on the frequency and magnitude of heavy precipitation, Nat. Hazards, 11, 283–303, doi:10.1007/BF00613411, 1995.

Fowler, H. J., Blenkinsop, S., and Tebaldi, C.: Review linking climate change modelling to impacts studies: recent advances in downscaling techniques for hydrological modelling, Int. J. Climatol., 27, 1547–1578, doi:10.1002/joc.1556, 2007.

Furrer, E. M. and Katz, R. W.: Improving the simulation of extreme precipitation events by stochastic weather generators, Water Resour. Res., 44, W12439, doi:10.1029/2008WR007316, 2008.

Gregersen I. B., Sørup H. J. D., Madsen H., Rosbjerg D., Mikkelsen P. S., and Arnbjerg-Nielsen K.: Assessing future climatic changes of rainfall extremes at small spatio-temporal scales, Climatic Change, 118, 783–797, doi:10.1007/s10584-012-0669-0, 2013.

Hazeleger, W., Wang, X., Severijns, C., Ştefănescu, S., Bintanja, R., Sterl, A., Wyser, K., Semmler, T., Yang, S., van den Hurk, B., van Noije, T., van der Linden, E., and van der Wiel, K.: EC-Earth V2.2: description and validation of a new seamless earth system prediction model, Clim. Dynam., 39, 2611–2629, doi:10.1007/s00382-011-1228-5, 2012.

Hundecha, Y., Pahlow, M., and Schumann, A.: Modeling of daily precipitation at multiple locations using a mixture of distributions to characterize the extremes, Water Resour. Res., 45, W12412, doi:10.1029/2008WR007453, 2009.

Jørgensen, H. K., Rosenørn, S., Madsen, H., and Mikkelsen, P. S.: Quality control of rain data used for urban runoff systems, Water Sci. Technol., 37, 113–120, doi:10.1016/S0273-1223(98)00323-0, 1998.

Kendon, E. J., Roberts, N. M., Fowler, H. J., Roberts, M. J., Chan, S. C., and Senior, C. A.: Heavier summer downpours with climate change revealed by weather forecast resolution model, Nat. Climate Change, 4, 570–576, 2014.

Larsen, A. N., Gregersen, I. B., Christensen, O. B., Linde, J. J., and Mikkelsen, P. S.: Potential future increase in extreme precipitation events over Europe due to climate change, Water Sci. Technol., 60, 2205–2216, doi:10.2166/wst.2009.650, 2009.

Madsen, H., Mikkelsen, P. S., Rosbjerg, D., and Harremoes, P.: Regional estimation of rainfall intensity-duration-frequency curves using generalized least squares regression of partial duration series statistics, Water Resour. Res., 38, 21-1–21-11, doi:10.1029/2001WR001125, 2002.

Madsen, H., Arnbjerg-Nielsen, K., and Mikkelsen, P. S.: Update of regional intensity-duration-frequency curves in Denmark: tendency towards increased storm intensities, Atmos. Res., 92, 343–349, doi:10.1016/j.atmosres.2009.01.013, 2009.

Maraun, D., Wetterhall, F., Ireson, A. M., Chandler, R. E., Kendon, E. J., Widmann, M., Brienen, S., Rust, H. W., Sauter, T., Themeßl, M., Venema, V. K. C., Chun, K. P., Goodess, C. M., Jones, R. G., Onof, C., Vrac, M., and Thiele-Eich, I.: Precipitation downscaling under climate change: recent developments to bridge the gap between dynamical models and the end user, Rev. Geophys., 48, RG3003, doi:10.1029/2009RG000314, 2010.

Mayer, S., Maule, C. F., Sobolowski, S., Bøssing, O. B., Sørup, H. J. D., Sunyer, M., Arnbjerg-Nielsen, K., and Barstad, I.: Added value from high-resolution mini-ensemble climate simulations over Scandinavia?, Tellus A, 67, 24941, doi:10.3402/tellusa.v67.24941, 2015.

Mikkelsen, P. S., Madsen, H., Rosbjerg, D., and Harremoes, P.: Properties of extreme point rainfall.3. Identification of spatial inter-site correlation structure, Atmos. Res., 40, 77–98, doi:10.1016/0169-8095(95)00026-7, 1996.

Mikkelsen, P. S., Madsen, H., Arnbjerg-Nielsen, K., Jørgensen, H. K., Rosbjerg, D., and Harremoës, P.: A rationale for using local and regional point rainfall data for design and analysis of urban storm drainage systems, Water Sci. Technol., 37, 7–14, 1998.

Nguyen, V.-T.-V., Nguyen, T.-D., and Ashkar, F.: Regional frequency analysis of extreme rainfalls, Water Sci. Technol., 45, 75–81, 2002.

Olsson, J., Berggren, K., Olofsson, M., and Viklander, M.: Applying climate model precipitation scenarios for urban hydrological assessment: a case study in Kalmar City, Sweden, Atmos. Res., 92, 364–375, doi:10.1016/j.atmosres.2009.01.015, 2009.

Roeckner, E., Bäuml, G., Bonaventura, L., Brokopf, R., Esch, M., Giorgetta, M., Hagemann, S., Kirchner, I., Kornblueh, L., Manzini, E., Rhodin, A., Schlese, U., Schulzweida, U., and Tompkins, A.: The atmospheric general circulation model ECHAM5: Model description, Max Planck Institute for Meteorology, Hamburg, Germany, Rep. 349, 140 pp., 2003.

HESSD
12, 2561–2605, 2015

Downscaling future precipitation extremes to urban hydrology scales

H. J. D. Sørup et al.

Rodriguez-Iturbe, I., Cox, D. R., and Isham, V.: Some models for rainfall based on stochastic point processes, Proc. Roy. Soc. A-Math. Phy., 410, 269–288, doi:10.1098/rspa.1987.0039, 1987a.
Rodriguez-Iturbe, I., Febres de Power, B., and Valdes, J. B.: Rectangular pulses point process models for rainfall: analysis of empirical data, J. Geophys. Res., 92, 9645–9656, doi:10.1029/JD092iD08p09645, 1987b.
Scharling, M.: Klimagrid Danmark nedbør 10 × 10 km (ver.2) – metodebeskrivelse, Danish Meteorological Institute, Copenhagen, Denmark, Technical Report No. 99-15, 1999 (in Danish).
Scharling, M.: Climate Grid Denmark, Danish Meteorological Institute, Copenhagen, Denmark, Technical Report No. 12-10, 2012.
Schilling, W.: Rainfall data for urban hydrology: what do we need?, Atmos. Res., 27, 5–22, doi:10.1016/0169-8095(91)90003-F, 1991.
Skamarock, W., Klemp, J., Dudhia, J., Gill, D., and Barker, D.: A description of the Advanced Research WRF version 3, National Center for Atmospheric Research, Boulder, CO, USA, NCAR Tech. Note NCAR/TN-475+STR, 113, doi:10.5065/D68S4MVH, 2005.
Sunyer, M. A., Madsen, H., and Ang, P. H.: A comparison of different regional climate models and statistical downscaling methods for extreme rainfall estimation under climate change, Atmos. Res., 103, 119–128, doi:10.1016/j.atmosres.2011.06.011, 2012.
Sunyer, M. A., Sørup, H. J. D., Christensen, O. B., Madsen, H., Rosbjerg, D., Mikkelsen, P. S., and Arnbjerg-Nielsen, K.: On the importance of observational data properties when assessing regional climate model performance of extreme precipitation, Hydrol. Earth Syst. Sci., 17, 4323–4337, doi:10.5194/hess-17-4323-2013, 2013.
Sunyer, M. A., Gregersen, I. B., Rosbjerg, D., Madsen, H., Luchner, J., and Arnbjerg-Nielsen, K.: Comparison of different statistical downscaling methods to estimate changes in hourly extreme precipitation using RCM projections from ENSEMBLES, Int. J. Climatol., doi:10.1002/joc.4138, online first, 2014a.
Sunyer, M. A., Madsen, H., Rosbjerg, D., and Arnbjerg-Nielsen, K.: A Bayesian approach for uncertainty quantification of extreme precipitation projections including climate model interdependency and non-stationary bias, J. Climate, 27, 7113–7132, doi:10.1175/JCLI-D-13-00589.1, 2014b.
Tebaldi, C. and Knutti, R.: The use of the multi-model ensemble in probabilistic climate projections, Philos. T. Roy. Soc. A, 365, 2053–2075, doi:10.1098/rsta.2007.2076, 2007.

HESSD
12, 2561–2605, 2015

Downscaling future precipitation extremes to urban hydrology scales

H. J. D. Sørup et al.

van der Linden, P. and Mitchell, J. F. B. (Eds.): ENSEMBLES: Climate Change and its Impacts: Summary of research and results from the ENSEMBLES project, Met Office Hadley Center, Exeter, 2009.

van Meijgaard, E., van Ulft, L. H., van de Berg, W. J., Bosveld, F. C., Hurk, B. J. J. M., Lenderink, G., and Siebesma, A. P.: The KNMI regional atmospheric climate model RACMO, version 2.1, Royal Dutch Meteorological Institute, De Bilt, the Netherlands, KNMI Technical Report No. 302, 2008.

van Vuuren, D. P., Edmonton, J., Kainuma, M., Riahi, K., Thomson, A., Hibbard, K., Hurtt, G. C., Kram, T., Krey, V., Lamarque, J.-F., Masui, T., Meinshausen, M., Nakocenovic, N., Smith, S. J., and Rose, S. K.: The representative concentration pathways: an overview, Climatic Change, 109, 5–31, doi:10.1007/s10584-011-0148-z, 2011.

Verhoest, N. E. C., Vandenberghe, S., Cabus, P., Onof, C., Meca-Figueras, T., and Jameleddine, S.: Are stochastic point rainfall models able to preserve extreme flood statistics?, Hydrol. Process., 24, 3439–3445, doi:10.1002/hyp.7867, 2010.

Vrac, M., Stein, M., and Hayhoe, K.: Statistical downscaling of precipitation through nonhomogeneous stochastic weather typing, Clim. Res., 34, 169–184, doi:10.3354/cr00696, 2007.

Waymire, E. and Gupta, V. K.: The mathematical structure of rainfall representations. I. A review of the stochastic rainfall models, Water Resour. Res., 17, 1261–1272, doi:10.1029/WR017i005p01261, 1981.

Wilks, D. S. and Wilby, R. L.: The Weather generator game: a review of stochastic weather models, Prog. Phys. Geog., 23, 329–357, doi:10.1177/030913339902300302, 1999.

Willems, P., Arnbjerg-Nielsen, K., Olsson, J., and Nguyen, V.-T.-V.: Climate change impact assessment on urban rainfall extremes and urban drainage: methods and shortcomings, Atmos. Res., 103, 106–118, doi:10.1016/j.atmosres.2011.04.003, 2012.

Wood, A. W., Leung, L. R., Sridhar, V., and Lettenmaier, D. P.: Hydrologic implications of dynamical and statistical approaches to downscaling climate model outputs, Climatic Change, 62, 189–216, doi:10.1023/B:CLIM.0000013685.99609.9e, 2004.

Table 1. Main characteristics of the two observational data sets used in this study.

	Type of data	Spatial data resolution	Temporal data resolution	Period
SVK	Point observations	60 stations	Minute data	1979–2012
CGD	Gridded data	10 km grid	Daily data	1989–2010

HESSD
12, 2561–2605, 2015

Downscaling future precipitation extremes to urban hydrology scales

H. J. D. Sørup et al.

Table 2. Regional Climate Model (RCM) runs from which precipitation output is used to calculate perturbations schemes for the WG used in this study. All have a temporal resolution of 1 h.

Name	RCM	GCM	Spatial resolution	Present period	Future period
HIRHAM SRES A1B	HIRHAM 5	ECHAM 5	25 km	1980–2009	2070–2099
RACMO SRES A1B	RACMO 2.1	ECHAM 5	25 km	1980–2009	2070–2099
HIRHAM rcp 4.5	HIRHAM 5	EC-EARTH	8 km	1981–2010	2071–2100
HIRHAM rcp 8.5	HIRHAM 5	EC-EARTH	8 km	1981–2010	2071–2100
WRF rcp 4.5	WRF 3	NorESM	8 km	1981–2010	2071–2100
WRF rcp 8.5	WRF 3	NorESM	8 km	1981–2010	2071–2100

HESSD
12, 2561–2605, 2015

Table 3. The relative weights used in the fitting procedure.

Statistic	Relative weight
24 h mean	1
24 h variance	3
24 h skewness	6
1 h variance	3
1 h skewness	6
1 h auto-correlation	6
1 h Cross-correlation	6*
Probability of dry day	1
Probability of dry hour	1

* All the cross-correlations of a gauge have equal weights that sum up to the value shown.

HESSD
12, 2561–2605, 2015

Table 4. e-folding distances for the SVK and WG maximum averaged intensities of extremes for 1, 6, 12 and 24 h duration, based on the fitted exponential models (cf. Fig. 8) as well as for a regional climate model (HIRHAM/ECHAM) from the study by Gregersen et al. (2013) for comparison.

e-folding distance [km]	1 h	6 h	12 h	24 h
SVK	3.5	5.5	7.3	8.
WGs	7.1–9.9	9.1–14	9.5–16	10–28
HIRHAM/ECHAM*	56	48	48	54

* Values from Gregersen et al. (2013).

HESSD
12, 2561–2605, 2015

Table 5. e-folding distances for all aggregation periods for all WG output.

e-folding distance [km]	Aggregation period			
	1 h	6 h	12 h	24 h
WG – Present Climate	3.9	5.0	4.9	5.0
WG – HIRHAM SRES A1B	5.2	7.4	7.7	8.1
WG – RACMO SRES A1B	7.3	9.7	9.1	8.4
WG – HIRHAM rcp 4.5	5.2	8.4	8.7	8.8
WG – HIRHAM rcp 8.5	4.6	7.7	9.3	9.0
WG – WRF rcp 4.5	5.1	9.1	9.3	11.5
WG – WRF rcp 8.5	4.9	9.4	9.9	10.2

HESSD
12, 2561–2605, 2015

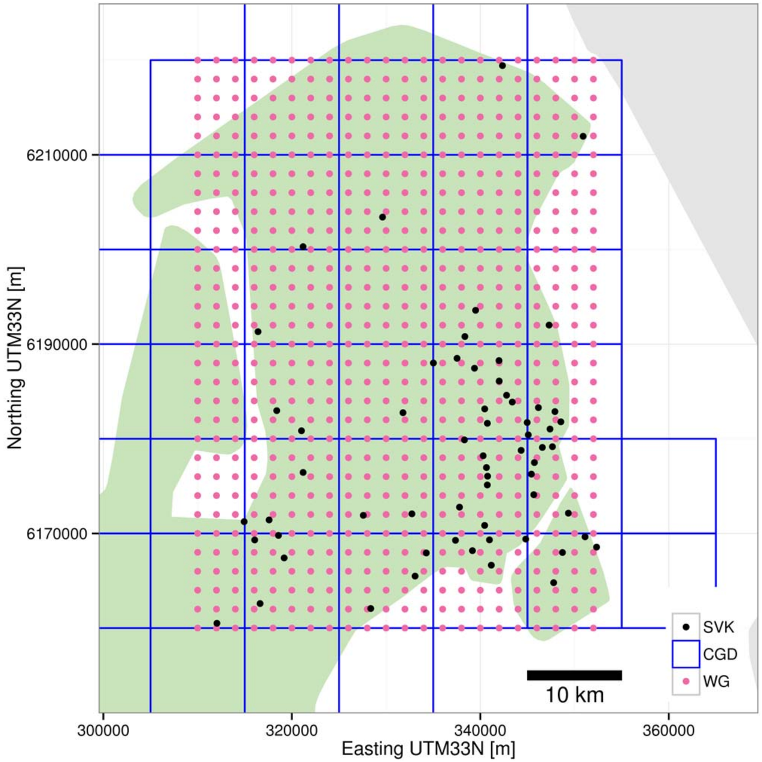

Figure 1. Locations of the rain gauges (SVK), the gridded data set (CGD) and extent of the modelled grid (WG) in the North-Eastern part of Zealand (Denmark) including Copenhagen in the South-Eastern part of the map where the concentration of SVK gauges is highest.

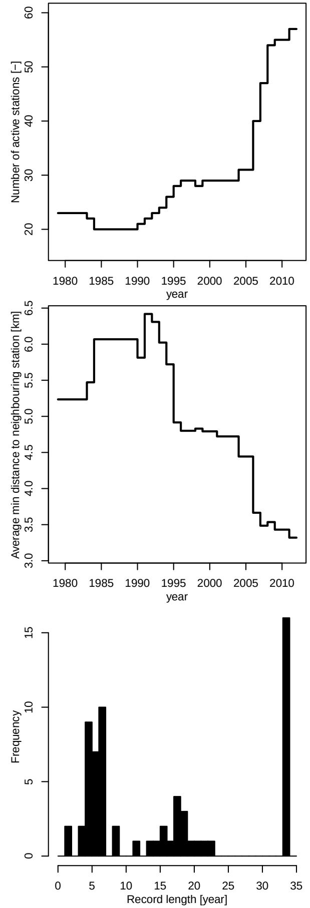

Figure 2. Temporal development in (top) the number of stations in the SVK data set and (middle) the average distance between closest neighbouring stations, and (bottom) the distribution of record lengths.

HESSD
12, 2561–2605, 2015

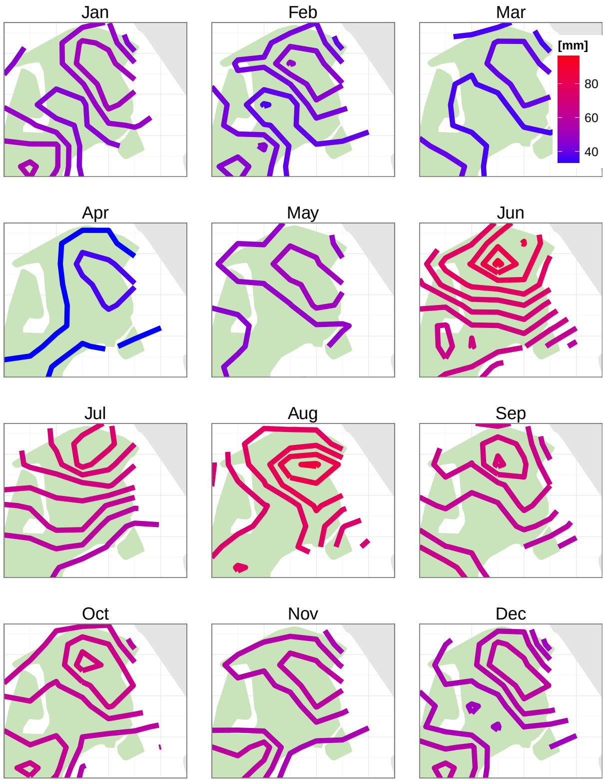

Figure 3. Spatial variation of the mean monthly precipitation calculated from the CGD data set for the model area.

HESSD
12, 2561–2605, 2015

Downscaling future precipitation extremes to urban hydrology scales

H. J. D. Sørup et al.

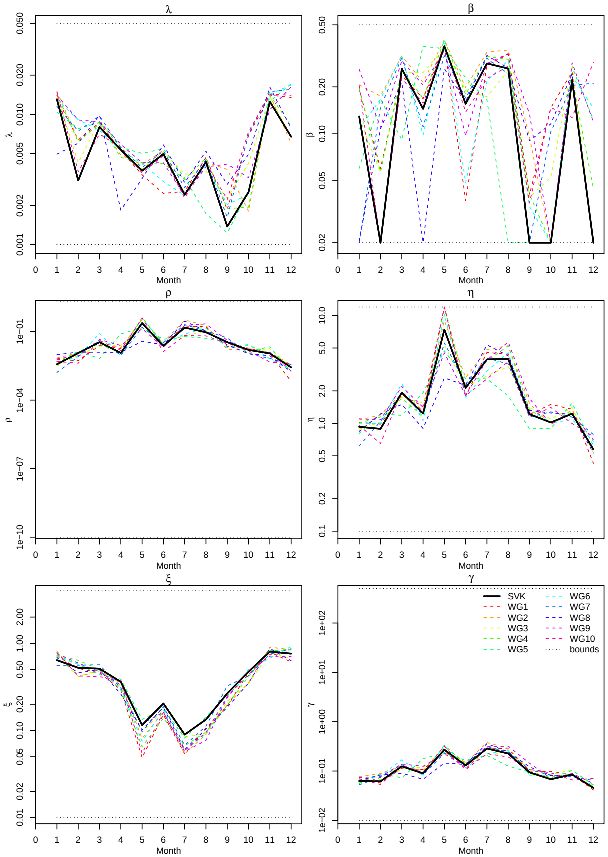

Figure 4. Monthly variation of the model parameters estimated from the SVK data set and from the simulated 10 WG data sets. Upper and lower fitting bounds are shown in light grey.

HESSD
12, 2561–2605, 2015

Downscaling future precipitation extremes to urban hydrology scales

H. J. D. Sørup et al.

Title Page
Abstract
Introduction
Conclusions
References
Tables
Figures
◀I
▶I
◀
▶
Back
Close
Full Screen / Esc
Printer-friendly Version
Interactive Discussion

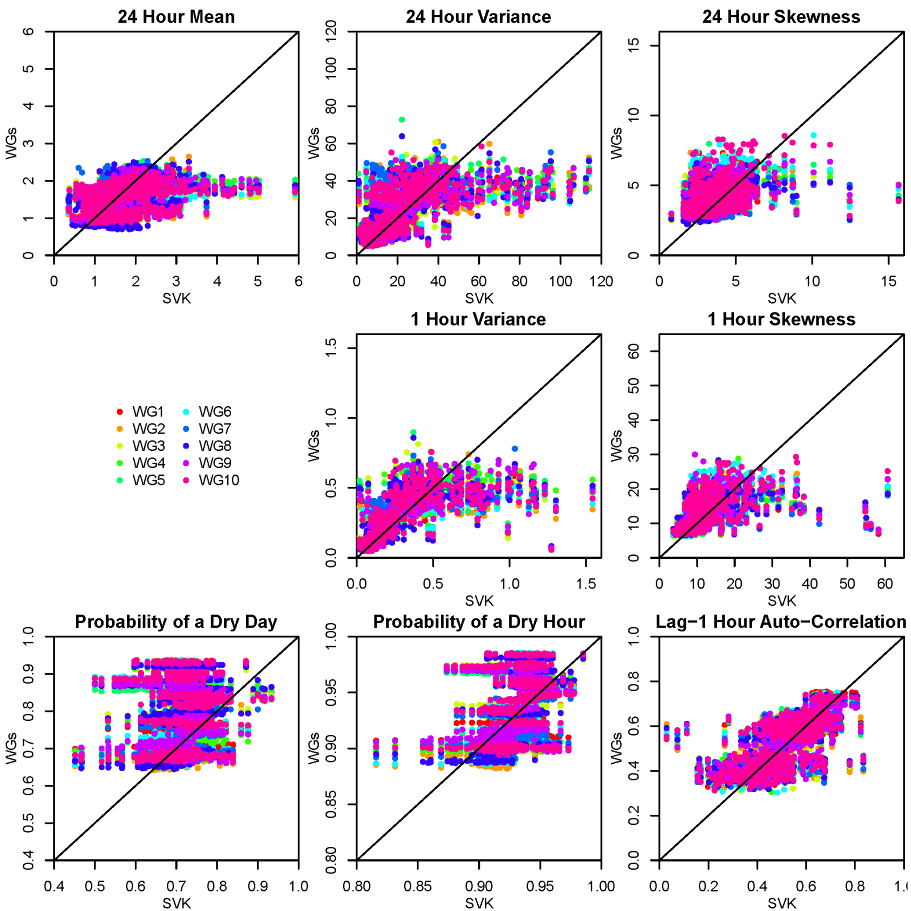

Figure 5. Fitting statistics calculated from the SVK data set (observations) and WG (simulated) data set.

HESSD
12, 2561–2605, 2015

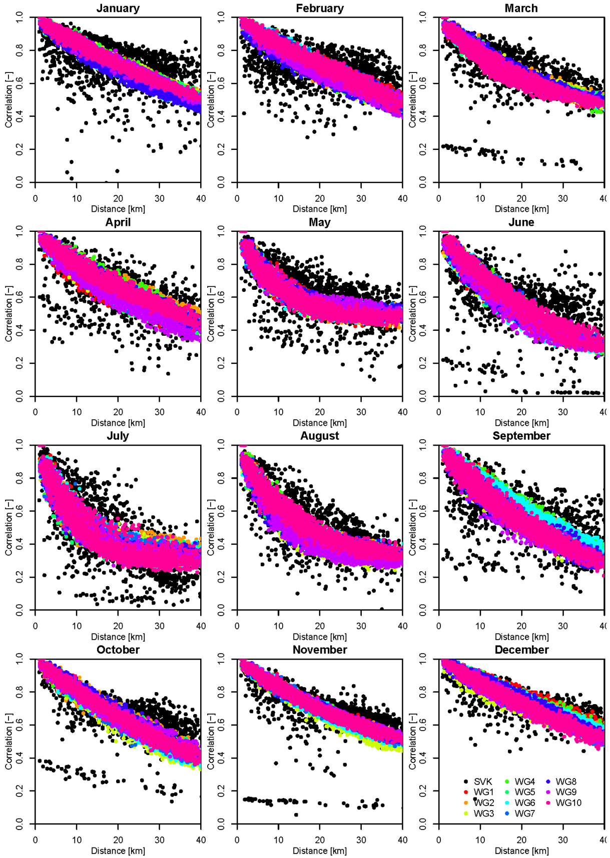

Figure 6. Variation of cross-correlation of the 1 h intensity with distance between pairs of gauges in the SVK data set (black dots) and grid points in the WG data set (coloured dots).

HESSD
12, 2561–2605, 2015

Downscaling future precipitation extremes to urban hydrology scales

H. J. D. Sørup et al.

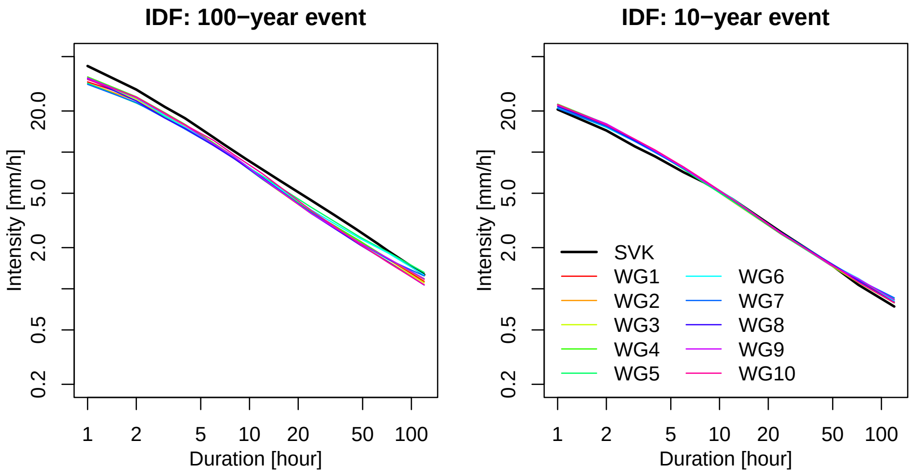

Figure 7. Mean intensity-duration-frequency curves for 100 and 10 year return periods calculated from the SVK data set and for all 10 WG realisations.

HESSD
12, 2561–2605, 2015

Downscaling future precipitation extremes to urban hydrology scales

H. J. D. Sørup et al.

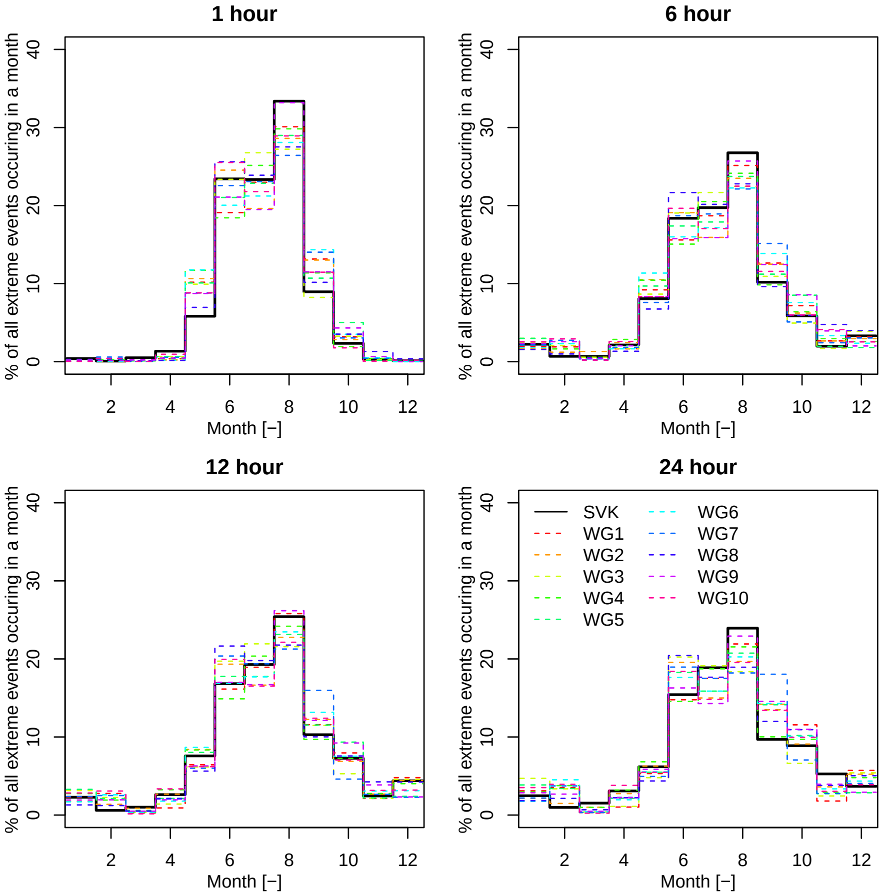

Figure 8. Monthly variation for 1, 6, 12 and 24 h durations of the frequency of extreme events in the SVK and WG data sets.

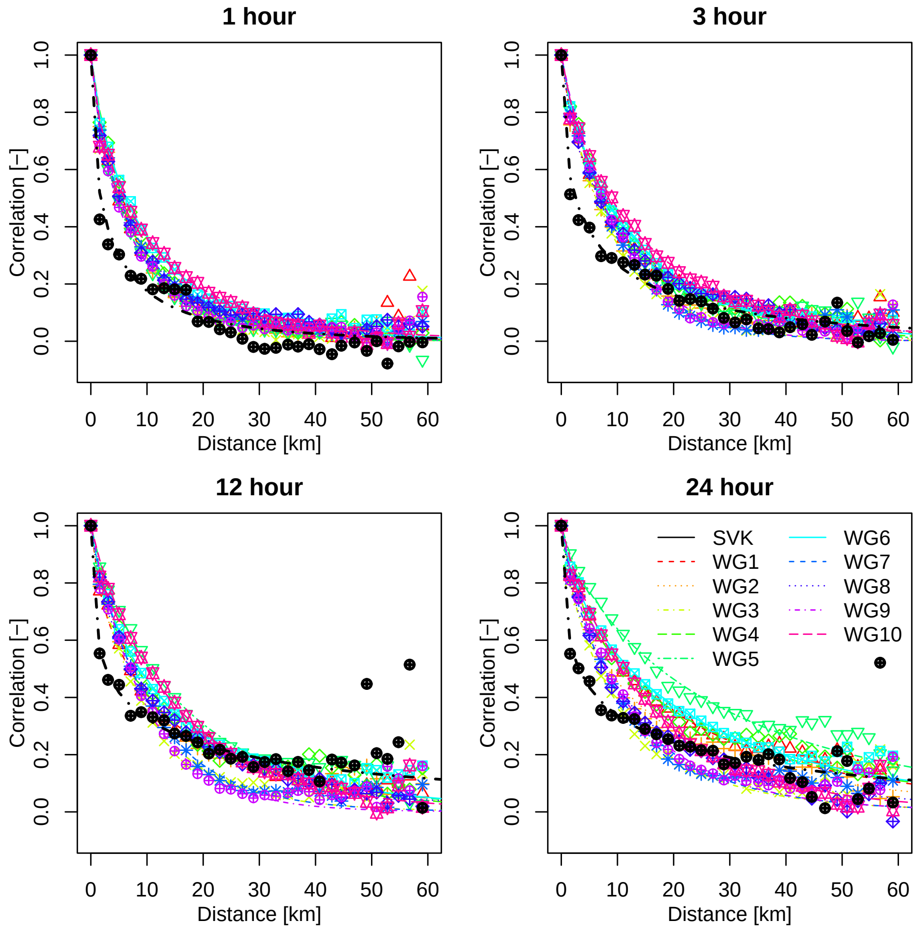

Figure 9. Unconditional spatial correlation for the SVK and WG data sets, calculated from maximum averaged intensities of extreme events for 1, 6, 12 and 24 h duration. Fitted exponential models that highlight overall tendencies are shown.

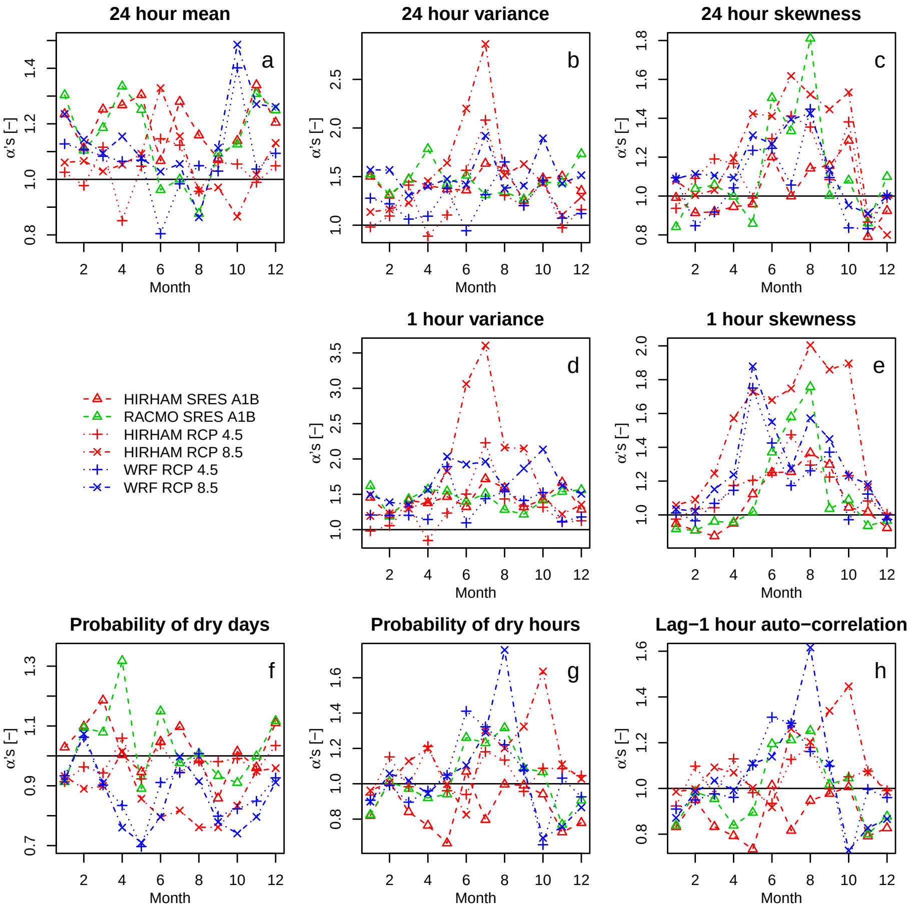

Figure 10. Climate factors, α's, calculated on a monthly basis for each statistic and each RCM. Each set of α's from an RCM act as a perturbation scheme for the WG.

HESSD
12, 2561–2605, 2015

Downscaling future precipitation extremes to urban hydrology scales

H. J. D. Sørup et al.

Title Page
Abstract | Introduction
Conclusions | References
Tables | Figures
◀I | ▶I
◀ | ▶
Back | Close
Full Screen / Esc
Printer-friendly Version
Interactive Discussion

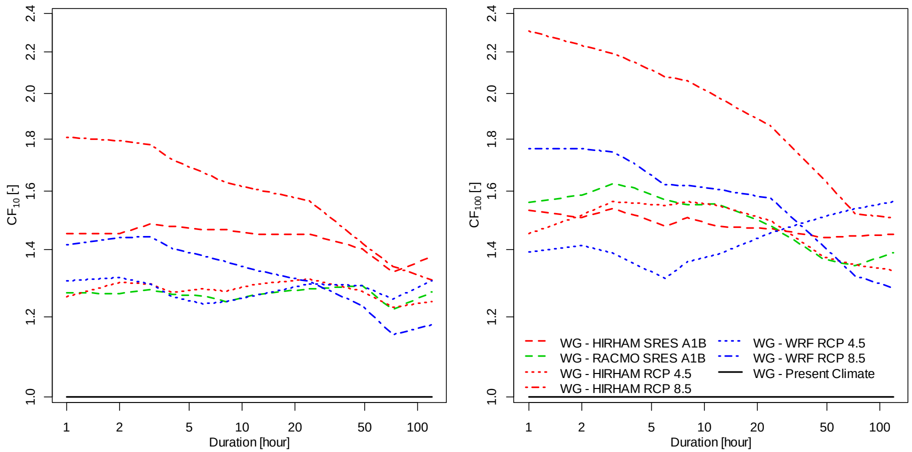

Figure 11. Climate change factors for different return periods for the different perturbed WG runs. T = 10 years (left) and T = 100 years (right).

HESSD
12, 2561–2605, 2015

Downscaling future precipitation extremes to urban hydrology scales

H. J. D. Sørup et al.

Title Page
Abstract | Introduction
Conclusions | References
Tables | Figures
◀| |▶
◀ ▶
Back | Close
Full Screen / Esc
Printer-friendly Version
Interactive Discussion

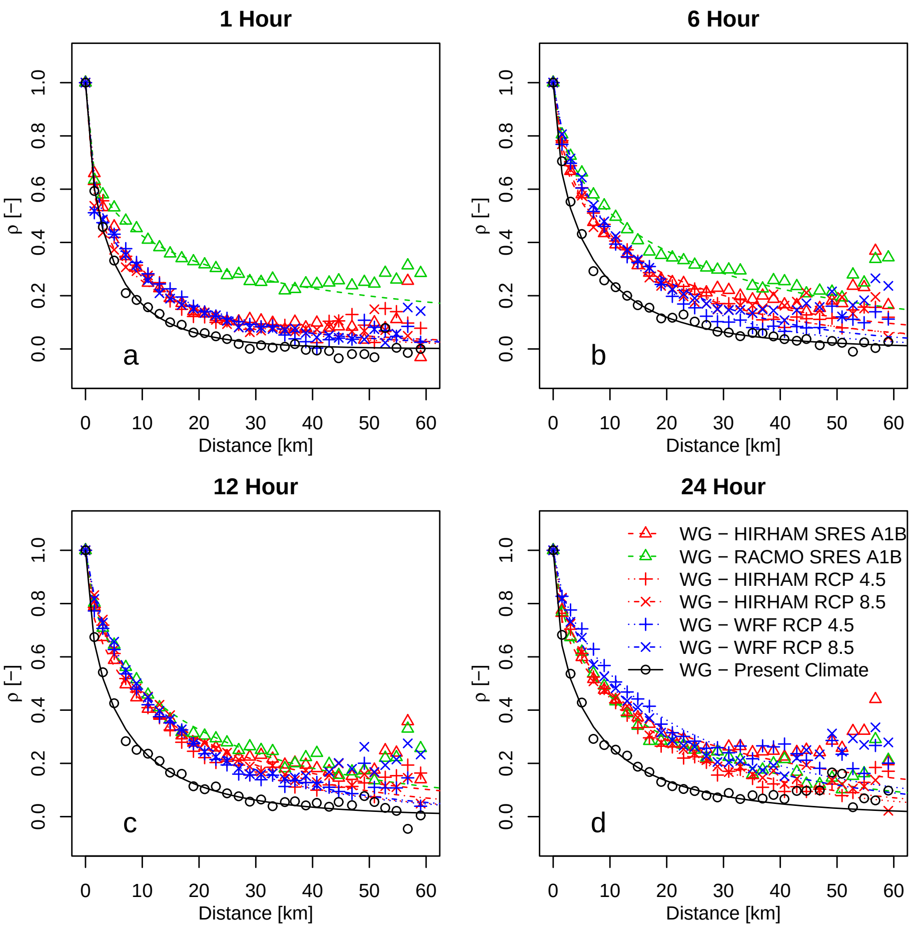

Figure 12. The unconditional spatial correlation of all *T*-year events for perturbed WG output for event durations of 1, 6, 12 and 24 h.